

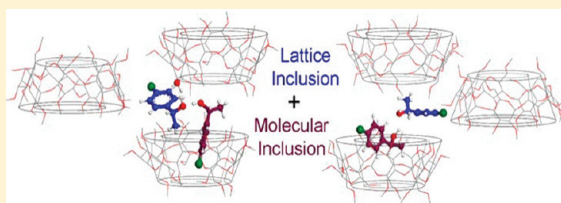
A Hybrid Mechanism in Chiral Discrimination Induced by Crystallization of Supramolecular Compounds

Youness Amharar, Arnaud Grandey, [†] Morgane Sanselme, Samuel Petit,* and Gérard Coquerel

Unité de Cristallogénèse, Sciences et Méthodes Séparatives (SMS) - UPRES EA 3233, IRCOF IMR 4114, Université de ROUEN, Rue Tesnière, F-76821 Mont Saint-Aignan Cedex, France

 Supporting Information

ABSTRACT: Host–guest complexes formed in aqueous medium between permethylated β -cyclodextrin ($\text{TM}\beta\text{-CD}$) and racemic 1-(*p*-fluorophenyl)ethanol (*p*-F-PE) are studied. The crystalline complexes are characterized and their crystal structures are determined, revealing two sets of solid phases with specific abilities for chiral discrimination: on the one hand, a stable complete solid solution with two independent complexes per asymmetric unit exhibits a limited chiral recognition, and on the other hand, two metastable partial solid solutions with unusual 1:2 host–guest stoichiometries behave as diastereomeric complexes. The structural features of the 1:2 complexes and their study by means of molecular modeling show that these solid phases, described as cocrystals formed between one host–guest inclusion complex and one non-engulfed *p*-F-PE molecule, present a significant chiral discrimination occurring both inside the cyclodextrin and outside the macrocycle in a crystal lattice cavity. Therefore, the enantioselectivity observed in this system results from an interplay between molecular inclusion in the cyclodextrin and lattice inclusion. To our knowledge, it is the first report of such a hybrid mechanism. An overview of the crystal structures of the literature containing $\text{TM}\beta\text{-CD}$ is also achieved and allows their classification in four structural groups in relation to their crystal packing features.



1. INTRODUCTION

Among preparative methods leading to high enantiomeric purities, crystallization-based processes such as Pasteurian resolution and preferential crystallization¹ constitute efficient, convenient, and cost-effective techniques. However, an alternative route available at the laboratory scale consists of the crystallization of supramolecular complexes formed with chiral hosts such as bulky polyols,² dibenzoyl tartaric acid,³ tri-*o*-thymotide,⁴ and cyclodextrins (CD hereafter), the latter being the most widely used chiral agents for the formation of host–guest complexes.⁵ The underlying mechanism relies on the crystallization of two diastereomeric compounds involving weak interactions between host and guest molecules (hydrogen bonds, van der Waals forces, or hydrophobic interactions) and exhibiting different physical properties.^{6–9} In some cases, the crystal structure determination of these complexes has provided valuable data for the rationalization of supramolecular interactions and chiral discrimination mechanisms.^{10–14} Although most of these structural investigations involved complexes formed with native β -CD, it was highlighted by Harata that structural features could provide an explanation of the lower ability of native CDs for enantiodiscrimination, compared to permethylated CDs.¹³ Indeed, permethylation induces important conformational changes of macrocycles, and the absence of intramolecular hydrogen bonds in permethylated CDs results in a higher molecular flexibility. Thanks to the presumed “induced fit”, this characteristic may facilitate the molecular adjustments of the guest molecule inside the cavity, leading to a more efficient chiral recognition.^{13,15}

During the past decade, Grandey and co-workers have investigated the crystallization behavior of host–guest complexes formed between permethylated β -cyclodextrin (named $\text{TM}\beta\text{-CD}$ hereafter) and a homologous series of racemic *p*-halogenated derivatives of 1-phenylethanol (*p*-X-PE hereafter) chosen as model compounds. These studies have revealed that enantioenrichments occurred for all of these derivatives but with a widespread range of diastereomeric excess values (de) in solid state samples.⁹ Using uniform experimental conditions (1:1 stoichiometry in aqueous medium), the resolution efficiency induced by crystallization was shown to be highly sensitive to kinetic parameters, since the de were, in most cases, strongly affected by crystallization durations. These diastereomeric complexes are composed of one guest molecule per $\text{TM}\beta\text{-CD}$ host, which is the usual stoichiometry for most of the complexes described in the literature.^{10,13,14,16–19}

In order to reach a better understanding of crystallization behaviors and related discrimination mechanisms, Grandey et al. have further investigated the complexes formed between $\text{TM}\beta\text{-CD}$ and *p*-Br-PE enantiomers,²⁰ from which two diastereomeric complexes ($\text{TM}\beta\text{-CD}/(S)\text{-}p\text{-Br-PE}$ and $\text{TM}\beta\text{-CD}/(R)\text{-}p\text{-Br-PE}$) could be isolated and characterized in the solid state (thermal behavior and solubilities). Furthermore, the comparison of their crystal structures provided valuable data related to stereodifferentiation at a molecular level, in particular

Received: February 21, 2012

Revised: April 17, 2012

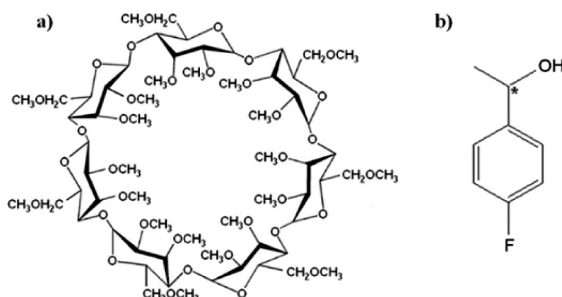
Published: April 17, 2012



different inclusion geometries of each guest enantiomer in the macrocycle and different crystal packings. Owing to the existence of a unique inclusion geometry in the solvated state with weak binding constants (determined by NMR studies) and to the occurrence of a complete solid solution for each of the two crystalline phases, it was stated that nucleation constitutes the key step that determines the nature of the diastereomeric compound obtained in the solid state.²¹ This study has also shown that an accurate control of crystallization conditions was a decisive requisite for the eventual preparative resolution of a racemic mixture by means of crystallization.

In the continuity of these investigations, the present paper reports the crystallization behavior, the physical characterization and the structure determination of complexes formed between 1-(*p*-fluorophenyl)ethanol (*p*-F-PE) and TM β -CD (Chart 1). This study revealed unexpected insights concerning the chiral discrimination mechanisms involved during the crystallization of these host–guest compounds.

Chart 1. Molecular Structures of TM β -CD (a) and *p*-F-PE (b)



2. EXPERIMENTAL SECTION

2.1. Materials. Commercial TM β -CD of high purity (>97%) was purchased from Cyclolab Inc. (Budapest, Hungary) and used without further purification. A racemic mixture and (*R*) enantiomer (98%ee) of *p*-F-PE were supplied by Fischer Scientific (Illkirch, France). (*S*)-*p*-F-PE (97%ee) was obtained from Sigma Aldrich (Lyon, France).

2.2. Preparation and Crystallization of Complexes. Crystalline complexes were obtained from aqueous solutions containing, in most cases, a (1:1) molar ratio of host and guest components (19 mg of *p*-F-PE and 190 mg of TM β -CD in 1.2 mL of water). After dissolution under magnetic stirring of TM β -CD in water at room temperature, the addition of *p*-F-PE induced the appearance of an emulsion caused by the weak miscibility of the two liquid phases. This emulsion disappeared progressively, and the complete homogeneity was observed after about 1 h, indicating the probable formation of solvated supramolecular entities. Because of the retrograde solubility of complexes formed with TM β -CD, crystallizations were induced by heating these solutions to 30 °C (± 0.5 °C, using a programmable cryo-thermostat). The suspensions were then maintained under magnetic stirring until filtration, which were performed at the crystallization temperature. Growth of single crystals was carried out within 3 days by slowly heating solutions—initially saturated at 25 °C—up to 30 °C at the 2 °C/day rate.

2.3. ^1H NMR Measurements. Host–guest stoichiometries were established by ^1H NMR spectroscopy performed in CDCl_3 on a Bruker AC 300 spectrometer. The binding

constants were determined by ^1H NMR titration experiments in D_2O . The TM β -CD concentration was kept constant (3×10^{-2} M) while the *p*-F-PE concentration was increased from 3×10^{-3} to 3×10^{-2} M and the chemical shifts of the TM β -CD protons were recorded at each concentration. The obtained ^1H NMR data were analyzed by the Rose–Drago method.²²

2.4. Chiral Gas Chromatography Analysis. Enantiomeric excesses (ee) of *p*-F-PE were determined by chiral gas chromatography analyses. The latter were performed on a Packard 5890 instrument equipped with a Supelco Betadex column (413 K isothermal run, injector and detector temperature 523 K, helium carrier gas, $\mu_{\text{opt}} = 30 \text{ cm s}^{-1}$). In order to avoid injection of TM β -CD, which can undergo pyrolysis in analytical conditions, host and guest components were first separated by means of preparative thin layer chromatography (eluant = ethyl acetate/chloroform (30:70); $R_f(p\text{-F-PE}) = 0.6$; $R_f(\text{TM}\beta\text{-CD}) = 0.1$).

2.5. Thermal Analysis. TG-DSC measurements were carried out by using a Netzsch STA 449C Jupiter apparatus (Selb, Germany). The purge gas was helium (flow = 40 mL/min), and the reference material was an empty covered aluminum pan. The samples were weighed in covered pierced aluminum pans, and then placed in the analyzer. Analyses were performed in the temperature range 20–180 °C using a 5 K·min⁻¹ heating rate. After acquisition, the PROTEUS software was used for data processing (v. 4.8.4, 2007). Hot stage microscopy analyses were performed using a Nikon microscope fitted with a Linkam hot-stage. A small amount of sample was placed on the sample stage and heated in the 20–180 °C temperature range at a rate of 5 K·min⁻¹.

2.6. Solubility Study. Phase solubility studies were carried out by a gravimetric method. Aqueous suspensions containing a (1:1) molar ratio of host and guest components were stirred at a controlled temperature for 12 h to reach equilibrium. The liquid and solid phases were separated by filtration. The nature of crystalline phases was determined by XRPD, and the saturated solution was weighed before and after complete evaporation of water.

2.7. X-ray Powder Diffraction. XRPD analyses were achieved with a D8 diffractometer (Bruker analytical X-ray Systems, Karlsruhe, Germany) with a Bragg–Brentano geometry, in theta–theta reflection mode. The instrument is equipped with an X-ray source ($\text{Cu}-\text{K}_{\alpha 1} = 1.5406 \text{ \AA}$, $\text{Cu}-\text{K}_{\alpha 2} = 1.5444 \text{ \AA}$, 40 kV, 40 mA), a nickel filter, and a lynx-eye detector with an angular aperture of 1.5°. Diffraction patterns were collected by steps of 0.04° (2-theta) over the angular range 3–30°, with a counting time of 0.5 s per step. PowderCell software was used for data processing (v 2.4, 2000).

2.8. Structural Investigations. Crystal structure determinations were carried out at room temperature and 100 K by means of single crystal X-ray diffraction on a full three-circle goniometer Bruker SMART APEX diffractometer equipped with a CCD area detector, using a monochromator for Mo K_{α} (0.7107 Å). In a preliminary step, the cell parameters and the orientation matrix of the crystal were determined by using SMART Software.²³ Data integration and global cell refinement were performed with SAINT software.²⁴ Intensities were corrected for Lorentz, polarization, decay, and absorption effects (SAINT and SADABS software) and reduced to F_O^2 . SHELX in the WinGX program package²⁵ was used for space group determination, structure solution (SHELXD),²⁶ and refinement (SHELXL).²⁷

2.9. Molecular Modeling. Molecular modeling calculations have been carried with the Materials Studio software (v5.5 Accelrys Inc.) starting from the structural data obtained by X-ray diffraction. Prior to energy calculations of host–guest interactions, each complex was submitted to geometry optimization by using the Dreiding forcefield in order to get reliable atomic charges by using the AM1 Hamiltonian (MOPAC). Then, the geometry optimization step was repeated, in which the electrostatic contribution could be taken into account. In order to ensure the validity of the procedure, every geometry-optimization step was systematically completed by a comparison with molecular conformations and host–guest inclusion geometries determined from X-ray diffraction. After the final energy minimization, the host and the guest were separated and their respective energies were calculated, from which the interaction energy could be estimated using the formula $E_{\text{interaction}} = E_{\text{host/guest}} - (E_{\text{host}} + E_{\text{guest}})$. Lattice energy calculations have also been performed using the same method for charge calculations and energy minimizations. Then, one guest molecule was replaced by its counter enantiomer, and the energy variations (intermolecular contributions) induced by the presence of this counter enantiomer in the structure were estimated by calculating the difference between the lattice energy of the simulated packing and that of the original one taken as a reference.

3. RESULTS AND DISCUSSION

3.1. Crystallization, Characterization, and Labels of Phases. Using racemic *p*-F-PE as a starting material, two crystalline phases have been obtained successively from the same supersaturated solution. The phase (X)-pss-O-1:2 (see Figure 1 for labels) crystallizes first, but maintaining the

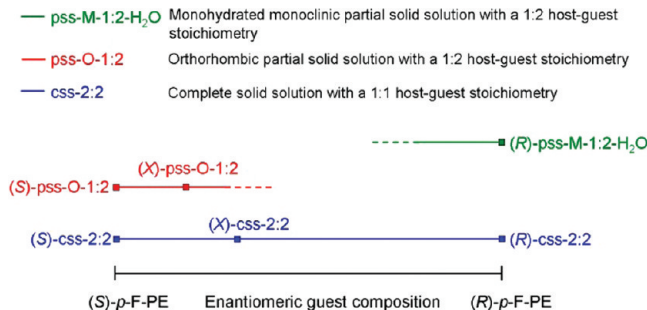


Figure 1. Scheme representing the solid phases observed in the water/*p*-F-PE/TM β -CD system as a function of the host–guest stoichiometry and the enantiomeric guest composition ($X = 82\%$ (S) for pss-O-1:2 and 67% (S) for css-2:2).

suspension under magnetic stirring for a few hours at 30 °C induces the appearance of (X)-css-2:2 while (X)-pss-O-1:2 dissolves. Identification by XRPD showed two distinct crystalline phases (Figure 2), and NMR analyses revealed a 1:1 stoichiometry for (X)-css-2:2 and a 1:2 TM β -CD:*p*-F-PE ratio for (X)-pss-O-1:2.

The same crystallization procedure was applied to an overall mixture with a 1:2 stoichiometry, leading then solely to the (X)-pss-O-1:2 crystalline phase. During this process, (X)-css-2:2 does not crystallize but the excess of *p*-F-PE induces the existence of a persistent emulsion caused by the lack of miscibility between the guest molecules and the aqueous solution. Similar behaviors were observed when crystallization experiments were performed using pure enantiomers of *p*-F-PE,

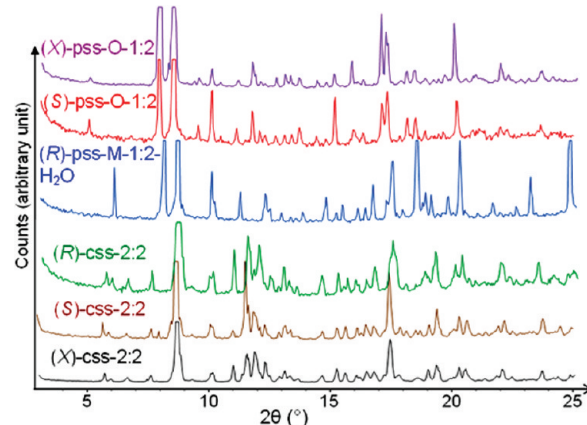


Figure 2. XRPD patterns of crystalline complexes obtained from solutions containing a 1:1 ratio of TM β -CD and (RS), (S), and (R) *p*-F-PE: (X)-pss-O-1:2, (S)-pss-O-1:2, (R)-pss-M-1:2-H₂O, (R)-css-2:2, (S)-css-2:2, and (X)-css-2:2.

and allowed the isolation and identification of four phases: (R)-css-2:2, (S)-css-2:2, (R)-pss-M-1:2-H₂O, and (S)-pss-O-1:2 (Figure 2). It will be shown in the next sections that the 1:1 solid phase actually consists of a complete solid solution containing two complexes per asymmetric unit, therefore labeled css-2:2. As a consequence, (R)-css-2:2, (S)-css-2:2, and (X)-css-2:2 denote the solid solution css-2:2 obtained from solutions containing pure (R)-*p*-F-PE, pure (S)-*p*-F-PE, and racemic *p*-F-PE, respectively. Along the same line, (R)-pss-M-1:2-H₂O, (S)-pss-O-1:2, and (X)-pss-O-1:2 exhibit a 1:2 host–guest stoichiometry and denote the monohydrated monoclinic partial solid solution pss-M-1:2-H₂O containing (R)-*p*-F-PE, the orthorhombic partial solid solution containing (S)-*p*-F-PE, and the same phase obtained from a solution containing a racemic guest composition, respectively. These labels are detailed in Figure 1. To our knowledge, these results constitute the first report, among crystallization studies involving TM β -CD, of the successive formation of two distinct crystalline phases and of the occurrence of a 1:2 stoichiometry.

3.2. Physical Characterization of Solid State Samples. The characterization of the different phases by TG-DSC revealed that (R)-css-2:2 and (S)-css-2:2 present similar thermal behaviors with a first endothermic event (onset: 133.2 °C for (R)-css-2:2 and 146.6 °C for (S)-css-2:2) combined with an exothermic peak (Figure 3). Hot stage microscopy observations have shown that these thermal events

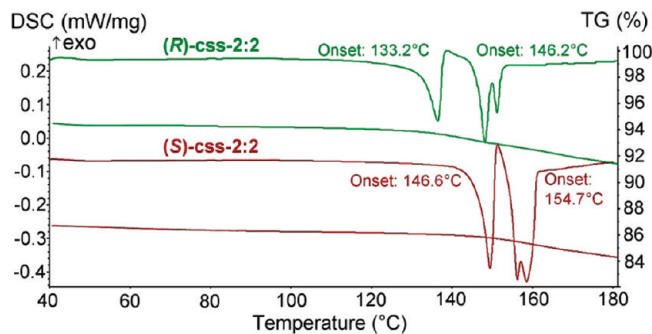


Figure 3. TG-DSC analysis of 1:1 crystalline complexes formed between TM β -CD and *p*-F-PE enantiomers: (R)-css-2:2 and (S)-css-2:2.

correspond to fusion-recrystallization phenomena (data not shown). Then, both phases (*R*)-css-2:2 and (*S*)-css-2:2 undergo fusion-degradation phenomena starting at 146.2 and 154.7 °C, respectively. The continuous mass losses detected from the thermogravimetric curves indicate that the first thermal event also triggers the partial and continuous evaporation of guest molecules. Owing to the higher temperature of successive events for (*S*)-css-2:2, it can also be deduced from TG-DSC analyses that the latter exhibits a higher thermal stability than (*R*)-css-2:2.

By contrast with the similarities depicted between (*R*)-css-2:2 and (*S*)-css-2:2, the TG-DSC analyses of (*R*)-pss-M-1:2-H₂O and (*S*)-pss-O-1:2 revealed distinct thermal profiles. As shown in Figure 4, (*R*)-pss-M-1:2-H₂O undergoes a first small

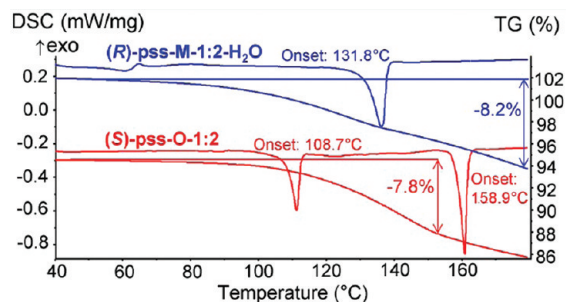


Figure 4. TG-DSC analysis of 1:2 crystalline complexes formed between TM β -CD and *p*-F-PE enantiomers: (*R*)-pss-M-1:2-H₂O and (*S*)-pss-O-1:2.

thermal event at ca. 60 °C. The concomitance of these small endo–exo phenomena with the beginning of a significant mass loss suggests that, beside dehydration, (*R*)-pss-M-1:2-H₂O undergoes a progressive release of the chiral guest. The destruction of the solid phase proceeds with a mass loss corresponding to half of a guest molecule (calculated mass per guest molecule: 8.2%) in the temperature range 60–130 °C and is completed by an endothermic event at 131.8 °C (onset temperature) associated with a melting of the remaining solid. The TG curve of (*S*)-pss-O-1:2 shows that, as for (*R*)-pss-M-1:2-H₂O, the mass starts to decrease at around 60–70 °C. The thermal profile presents two fusion-like phenomena at 108.7 and 158.9 °C. Further investigations (hot-stage microscopy) confirmed that the two endothermic peaks probably correspond to the fusion of different solid phases, but temperature-resolved XRPD also revealed the presence of a distinct XRPD pattern at ca. 90 °C that could not be identified as a known form of TM β -CD (hydrate, complex, or polymorph). Despite the reproducibility of these phenomena, a definitive interpretation of the DSC curve of (*S*)-pss-O-1:2 could not be achieved because of the chemical decomposition starting at ca. 60 °C. However, these analyses still highlight the distinct behaviors of (*R*)-pss-M-1:2-H₂O and (*S*)-pss-O-1:2, by contrast with the similarities depicted between (*R*)-css-2:2 and (*S*)-css-2:2.

The physical characterization of the new complexes was completed by solubility measurements performed in the temperature range 20–40 °C in aqueous solutions containing a 1:1 TM β -CD:*p*-F-PE ratio by using the gravimetric method (Figure 5). Since the compositions of (*R*)-pss-M-1:2-H₂O, (*S*)-pss-O-1:2, and (*X*)-pss-O-1:2 crystallized phases differ from that of their respective saturated solutions, the “true” solubilities cannot be measured, but metastable noncongruent

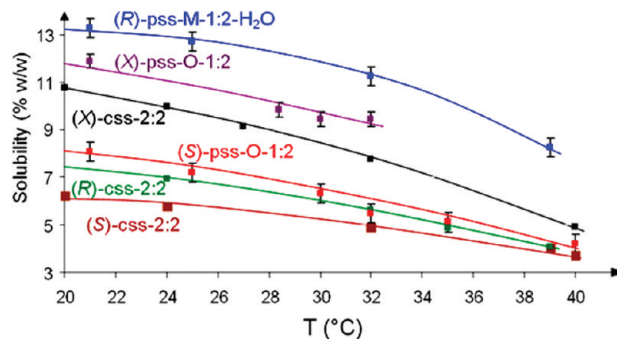


Figure 5. Solubility curves in water of crystalline complexes obtained from solutions containing a 1:1 ratio of TM β -CD and (RS), (S), and (R) *p*-F-PE: (*X*)-pss-O-1:2, (*S*)-pss-O-1:2, (*R*)-pss-M-1:2-H₂O, (*R*)-css-2:2, (*S*)-css-2:2, and (*X*)-css-2:2.

solubilities can be estimated. The six phases present similar slopes of solubility curves in water, characterized—likewise TM β -CD and the other TM β -CD complexes—by a retrograde behavior within the range of temperature investigated. It can be noticed that the diastereomerically pure phases containing the (*S*) guest enantiomer present the lowest solubilities. However, the solubility difference between (*R*)-css-2:2 and (*S*)-css-2:2 is small and decreases at higher temperature, whereas the solubility of (*R*)-pss-M-1:2-H₂O is larger by 4–5% w/w (i.e., ca. 60–80% more soluble) than that of (*S*)-pss-O-1:2 whatever the temperature. The discrepancy between the solubility curves and thermal profiles of (*S*)-pss-O-1:2 and (*R*)-pss-M-1:2-H₂O may be correlated to structural differences, as presumed from their XRPD patterns, whereas (*R*)-css-2:2 and (*S*)-css-2:2 may present structural analogies, owing to their similar XRPD patterns. It should also be noticed that (*X*)-pss-O-1:2 solubility is intermediate between that of (*S*)-pss-O-1:2 and (*R*)-pss-M-1:2-H₂O, whereas the presence of both enantiomers in (*X*)-css-2:2 results in a strongly enhanced solubility with reference to pure phases (*R*)-css-2:2 and (*S*)-css-2:2.

3.3. Structural Investigations. Six single crystals of the phases formed with enantiomerically pure guest molecules ((*R*)-css-2:2, (*S*)-css-2:2, (*R*)-pss-M-1:2-H₂O, and (*S*)-pss-O-1:2) and of compounds obtained from racemic solutions ((*X*)-css-2:2 and (*X*)-pss-O-1:2) could be grown by slow evaporation of supersaturated aqueous solutions with a 1:1 host–guest stoichiometry at 30 °C. The main data related to structure determinations at room temperature or at 100 K are collected in Table 1, and complete structural data have been deposited to the Cambridge Structural Database (CSD). The classification of structures containing TM β -CD initiated by Grandjean et al.²⁰ could therefore be updated by addition of these new results and of structures published since 2003. In the new inventory containing 36 entries (Table 2), the selected items (space group, crystallographic parameters) allowed the identification of four structural groups (instead of two in the previous version) corresponding to distinct crystal packings (Figure 6):

- SGA (space group $P_{2_1}2_12_1$): The crystal packing is made of 2-fold corrugated columns running along the crystallographic axis *b*. Molecular columns with a same orientation are stacked along the crystallographic axis *a* and, therefore, form a succession of antiparallel (002) layers.
- SGB (space group $P_{2_1}2_12_1$): Molecular columns are found along the crystallographic axis *a*, and are stacked along the *b* axis, resulting in the succession of (002)

Table 1. Crystallographic Data of the Crystal Structures of (S)-css-2:2, (X)-css-2:2, (R)-css-2:2, (S)-pss-O-1:2, (X)-pss-O-1:2, and (R)-pss-M-1:2-H₂O

	supramolecular complex code	TMβ-CD/(-)p-F-PE (S)-css-2:2	TMβ-CD/(±)p-F-PE (X)-css-2:2	TMβ-CD/(+)p-F-PE (R)-css-2:2	TMβ-CD/2(±)p-F-PE (S)-pss-O-1:2	TMβ-CD/2(−)p-F-PE (X)-pss-O-1:2	TMβ-CD/2(+p-F-PE (R)-pss-M-1:2-H ₂ O
formula	C ₆₃ H ₁₁₂ O ₃₅ ·C ₈ H ₉ OF	C ₆₃ H ₁₁₂ O ₃₅ ·C ₈ H ₉ OF	C ₆₃ H ₁₁₂ O ₃₅ ·C ₈ H ₉ OF	C ₆₃ H ₁₁₂ O ₃₅ ·C ₈ H ₉ OF	C ₆₃ H ₁₁₂ O ₃₅ ·(C ₈ H ₉ OF) ₂	C ₆₃ H ₁₁₂ O ₃₅ ·(C ₈ H ₉ OF) ₂	C ₆₃ H ₁₁₂ O ₃₅ ·(C ₈ H ₉ OF) ₂ ·H ₂ O
CSD refcode	867764	867765	867766	867767	867768	867769	867768
morphology	prismatic	prismatic	prismatic	rod-like	rod-like	rod-like	rod-like
color	colorless	colorless	colorless	colorless	colorless	colorless	colorless
molecular weight (g·mol ⁻¹)	1569.7	1569.7	1569.7	1709.9	1709.9	1709.9	1727.9
T (K)	100	295	100	295	100	295	295
space group	P2 ₁	P2 ₁ ,2 ₁	P2 ₁ ,2 ₁				
a (Å)	10.568(1)	10.752(1)	10.587(1)	14.649(12)	14.5053(10)	11.964(1)	11.964(1)
b (Å)	52.168(3)	52.786(2)	52.327(3)	22.288(10)	21.9188(16)	28.732(2)	28.732(2)
c (Å)	16.145(1)	16.131(1)	15.966(1)	28.450(20)	28.260(2)	14.722(1)	14.722(1)
β (deg)	108.11(1)	108.42(1)	107.96(1)	90	90	90	112.27(1)
Z, Z'	4, 2	4, 2	4, 1	4, 1	4, 1	2, 1	2, 1
V (Å ³)	8460	8686	8414	9289	8985	4683	4683
D _{calc}	1.23	1.20	1.24	1.22	1.22	1.22	1.22
Nb of collected/unique reflections	67951/17456	55065/24550	67764/17257	344244/19110	15313	14503	12035
no. of reflections (I > 2σ(I))	9824	12263	6887	15313	15313	14503	14503
residual electronic density (e·Å ⁻³)	0.328/-0.268	0.449/-0.217	0.474/-0.373	0.894/-0.262	0.623/-0.415	0.812/-0.417	0.812/-0.417
no. of parameters	2047	1948	2009	1095	1124	1097	1097
R ₁ , wR ₂ (I > 2σ(I)) ^a	0.049, 0.108	0.055, 0.124	0.061, 0.142	0.119, 0.274	0.0731, 0.177	0.117, 0.313	0.117, 0.313
R ₁ , wR ₂ (all data)	0.094, 0.119	0.107, 0.144	0.146, 0.160	0.140, 0.288	0.093, 0.191	0.154, 0.347	0.154, 0.347
goodness of fit	0.859	0.826	0.780	1.29	1.05	1.15	1.15

^a R = Σ(|F_O| - |F_C|)/Σ|F_O|, wR₂ = [Σ[w(F_O² - F_C²)²]/Σ[w(F_O²)²]]^{1/2}.

Table 2. Classification of Crystal Structures Containing TM β -CD

guest	stoich	SG ^a	crystallographic parameters					packing ^b	θ^c (deg)	ref
			<i>a</i> (Å)	<i>b</i> (Å)	<i>c</i> (Å)	β (deg)				
SGA										
(S) naproxen	1:1	<i>P</i> 2 ₁ 2 ₁ 2 ₁	15.179	21.407	27.67	90	A2F (b)	3.5	14	
<i>p</i> -iodophenol	1:1:4H ₂ O	<i>P</i> 2 ₁ 2 ₁ 2 ₁	14.997	21.368	28.205	90	A2F (b)	4	16	
(R)-5-ethyl-5-(4'methylphenyl) hydantoin	1:1	<i>P</i> 2 ₁ 2 ₁ 2 ₁	14.854	21.383	28.509	90	A2F (b)	4.2	18	
fenothrothion	1:1	<i>P</i> 2 ₁ 2 ₁ 2 ₁	15.159	21.128	27.558	90	A2F (b)	0	19	
4-hydroxyazobenzene	1:1:6H ₂ O	<i>P</i> 2 ₁ 2 ₁ 2 ₁	14.845	22.171	27.544	90	A2F (b)	6.1	28	
(S) p-F-PEe	1:2	<i>P</i> 2 ₁ 2 ₁ 2 ₁	14.649	22.288	28.450	90	A2F (b)	0	T ^d	
suprofen	1:1	<i>P</i> 2 ₁ 2 ₁ 2 ₁	15.389	21.051	27.027	90	A2F (b)	4	29	
(S)-p-methoxyphenyl propylthiosulfinate	1:1	<i>P</i> 2 ₁ 2 ₁ 2 ₁	14.775	21.333	27.872	90	A2F (b)	4	30	
(Z) ajoene	1:1	<i>P</i> 2 ₁ 2 ₁ 2 ₁	15.102	21.520	27.313	90	A2F (b)	4	31	
(S) flurbiprofen	1:1	<i>P</i> 2 ₁ 2 ₁ 2 ₁	15.271	21.451	27.895	90	A2F (b)	4	32	
(R) flurbiprofen	1:1:H ₂ O	<i>P</i> 2 ₁ 2 ₁ 2 ₁	15.092	21.714	28.269	90	A2F (b)	5	32	
m-iodophenol	1:1	<i>P</i> 2 ₁ 2 ₁ 2 ₁	15.669	20.798	25.486	90	A2F (b)	26	33	
4-biphenyl acetic acid	1:1:H ₂ O	<i>P</i> 2 ₁ 2 ₁ 2 ₁	14.890	21.407	28.540	90	A2F (b)	5	33	
ethyl laurate	1:1:2H ₂ O	<i>P</i> 2 ₁ 2 ₁ 2 ₁	14.796	22.444	27.720	90	A2F (b)	5	34	
(S) ibuprofen	1:1	<i>P</i> 2 ₁ 2 ₁ 2 ₁	15.232	21.327	27.597	90	A2F (b)	4	35	
cycluron	1:1:0.9H ₂ O	<i>P</i> 2 ₁ 2 ₁ 2 ₁	14.887	21.244	27.933	90	A2F (b)	3.8	36	
SGB										
(S)-1,7-dioxaspiro (5.5) undecane	1:1:H ₂ O	<i>P</i> 2 ₁ 2 ₁ 2 ₁	10.936	25.53	29.64	90	AC (a)	21.4	10	
methyl cyclohexane	1:1	<i>P</i> 2 ₁ 2 ₁ 2 ₁	11.149	25.664	29.427	90	AC (a)	31	37	
(R)-5-ethyl-1,3,5-trimethyl hydantoin	1:1	<i>P</i> 2 ₁ 2 ₁ 2 ₁	11.149	25.664	29.427	90	AC (a)	31	38	
psoralen	1:1:H ₂ O	<i>P</i> 2 ₁ 2 ₁ 2 ₁	10.945	25.652	29.939	90	AC (a)	21	39	
endo-8-azibicyclo (3.2.1) octan-3-ol	1:1	<i>P</i> 2 ₁ 2 ₁ 2 ₁	11.188	25.291	29.152	90	AC (a)	33	40	
L-menthol	1:1:2H ₂ O	<i>P</i> 2 ₁ 2 ₁ 2 ₁	11.060	26.138	29.669	90	AC (a)	21	41	
4-amino azobenzene	1:1:H ₂ O	<i>P</i> 2 ₁ 2 ₁ 2 ₁	10.699	27.363	29.167	90	AC (a)	21	28	
CpFe(CO) ₂ Cl	1:1	<i>P</i> 2 ₁ 2 ₁ 2 ₁	11.189	25.149	28.964	90	AC (a)	33	42	
SGC										
indole-3-butric acid	1:1:0.37H ₂ O	<i>P</i> 2 ₁	11.411	28.629	15.069	111.9	AC (a)	22	17	
2,4-dichlorophenoxy acetic acid	1:1:2H ₂ O	<i>P</i> 2 ₁	11.68	28.23	15.02	112.6	AC (a)	25	17	
(R) p-F-PE ^e	1:2:H ₂ O	<i>P</i> 2 ₁	11.964	28.731	14.722	112.3	AC (a)	24	T ^d	
(E) ajoene	1:1:0.5H ₂ O	<i>P</i> 2 ₁	11.553	27.715	14.605	109.4	AC (a)	27	31	
SGD										
(R) p-Br-PE ^e	1:1	<i>P</i> 2 ₁	10.563	14.731	27.355	98.5	AC (a)	13	20	
4-aminobenzoic acid n-butyl ester	1:1:0.36H ₂ O	<i>P</i> 2 ₁	10.891	14.858	27.583	99.6	AC (a)	15	43	
miscellaneous										
(S) p-Br-PE ^e	1:1	<i>P</i> 2 ₁ 2 ₁ 2 ₁	15.113	15.223	35.876	90	HB	20		
(\pm)-p-F-PE ^e	2:2	<i>P</i> 2 ₁	10.752	52.786	16.131	108.4	AC (a)	37/4	T ^d	
Cp ₂ NbCl ₂	1:1:4H ₂ O	<i>P</i> 2 ₁	14.726	26.194	12.863	109.1	AC (a/c)	45/26	45	
monohydrated form	1:H ₂ O	<i>P</i> 2 ₁ 2 ₁ 2 ₁	14.818	19.362	26.510	90	HB	44		
trihydrated form	1:3H ₂ O	<i>P</i> 2 ₁ 2 ₁ 2 ₁	16.205	16.287	30.099	90	A2F (a)	21	46	
anhydrous form III		<i>P</i> 2 ₁ 2 ₁ 2 ₁	15.951	16.577	28.941	90	A2F (a)	17	46	
4-chlorophenoxy acetic acid	2:2	<i>P</i> 2 ₁	10.93	25.284	29.954	92.9	AC (a)	24/31	47	

^aSpace group. ^bA2F (*x*), antiparallel 2-fold corrugated column along the *x* direction; AC (*x*), antiparallel column along the *x* direction; HB, herringbone. ^c θ : angle between the pseudo-7 axis of the macrocycle and the direction of the column. ^d*T*: this work. ^ep-X-PE: 1-(*p*-halogenophenyl)ethanol.

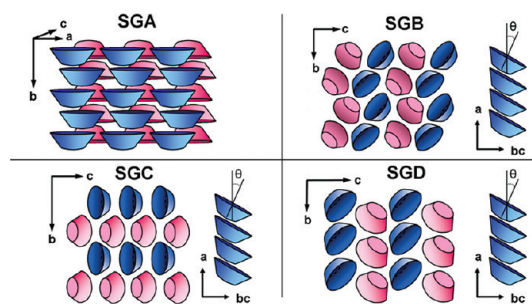


Figure 6. Schematic representation of the crystal packing in the four structural groups.

antiparallel layers. By contrast to SGA, the columns are shifted from one another by *c*/4 and therefore form a wavy slice instead of a true flat layer. Moreover, the macrocycles are tilted with reference to the *a* axis, and their pseudo-7-fold axis forms an angle of $\theta = 27 \pm 6^\circ$ with the column direction.

- SGC constitutes a new group and presents a monoclinic *P*2₁ symmetry. This structural type is characterized by molecular columns running along the crystallographic axis *a* and translated by *c*, resulting in a succession of antiparallel (020) layers along the *b* direction. The mean θ value is $24 \pm 3^\circ$.

- SGD is also composed of structures in the $P2_1$ space group and contains molecular columns along the a axis. However, in these structures, the stacking of these columns along b induces the existence of antiparallel (002) layers along the c axis, thus differing from the packing depicted in SGC. In this group, the mean θ value is $14 \pm 1^\circ$.

The three-dimensional packings of the six TM β -CD/*p*-F-PE crystal structures reported here were analyzed in the frame of this classification in order to facilitate the complete description of their structural features.

3.3.1. Crystal Structures of (R)-css-2:2, (X)-css-2:2, and (S)-css-2:2 Complexes. (R)-css-2:2, (X)-css-2:2, and (S)-css-2:2 exhibit similar crystallographic parameters and packing features, constituting therefore a unique structural type and raising a strong suspicion of solid solution between (R)-css-2:2 and (S)-css-2:2. The limited variations of unit cell parameters can be accounted for by differences in enantiomeric composition and also by the thermal expansion between 100 K ((R)-css-2:2 and (S)-css-2:2) and 298 K ((X)-css-2:2). A satisfying quality of structural determinations has been reached whatever the temperature, as shown from the various indicators listed in Table 1. Owing to its original features, this crystal packing does not enter in any of the four structural groups depicted above, and its most striking characteristic is the presence of two complexes per asymmetric unit, labeled H_A-G_A and H_B-G_B (Figure 7). This unusual feature has been observed only once, namely, in the structure of the complex formed between TM β -CD and 4-chlorophenoxyacetic acid.⁴⁷

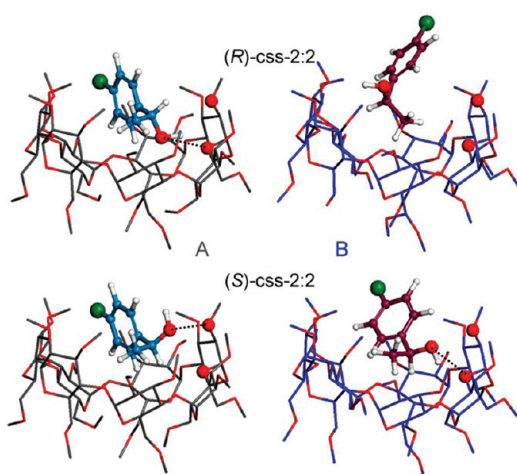


Figure 7. Complexes A (gray and cyan) and B (blue and purple) in the structures (R)-css-2:2 (upper) and (S)-css-2:2 (lower). The orientation of the macrocycles has been fixed so as to ease the visualization of inclusion geometries. Hydrogen atoms of TM β -CD are omitted for clarity.

Surprisingly the macrocycle conformations of the two independent TM β -CD molecules are similar, as shown from the tilt angle values for H_A and H_B (see the Supporting Information). Furthermore, the tilt angle values do not strongly depart from that reported in most structures (which means that the concept of induced fit is actually poorly applicable), and the only significant differences in terms of molecular geometry are related to the orientation of the methoxy groups. Therefore, it cannot be stated that the conformational features of TM β -CD molecules are responsible for the existence of two complexes in

the asymmetric unit. In previously reported structures of complexes formed between small aromatic guests and TM β -CD, the phenyl moiety is most often deeply engulfed in the cavity of the macrocycle. The structures of (R)-css-2:2, (S)-css-2:2, and (X)-css-2:2 constitute the second exception to this rule, since, as in the structure of TM β -CD/(S)-*p*-Br-PE,²⁰ the halogen atoms are either lying on the upper rim of the macrocycle (H_A-G_A) or even located outside the macrocycle (H_B-G_B), inducing that phenyl groups are poorly engulfed in TM β -CD cavities. It can be seen from Figure 7 that, in complexes A, the two guest enantiomers ((R)-G_A and (S)-G_A) have a similar location relative to H_A and this inclusion geometry was previously depicted in the complex TM β -CD/(S)-*p*-Br-PE,²⁰ with the alcohol moiety slightly inside the cavity.

The accommodation of the stereogenic center for each of the two enantiomers imposes different orientations of the alcohol function, inducing that hydrogen bonds between guest molecules and macrocycles are formed with different acceptors of the host: for the (S) enantiomer, the alcohol function is linked to a secondary methoxy group with a distance of 2.86 Å between the two oxygen atoms, whereas the hydrogen bond between the (R) enantiomer and the macrocycle involves an oxygen atom O4 ($d_{O-O} = 2.79$ Å). This hydrogen bond feature is quite unusual, and was previously observed only in the structure of the complex formed between TM β -CD and *endo*-8-azibicyclo[3.2.1]octan-3-ol.³⁹ In complexes B, different inclusion geometries are observed, depending on the stereochemistry of the guests. (S)-G_B, like (S)-G_A and (R)-G_A, is more deeply engulfed in the macrocycle, inducing that van der Waals contacts with the host are reinforced by a hydrogen bond with an ether function of the TM β -CD ($d_{O-O} = 2.96$ Å). By contrast, (R)-G_B is mainly located outside the cavity, so no hydrogen bond exists with the host, since the only methoxy group in the vicinity of the guest hydroxyl function is not close enough to form a bond ($d_{O-O} = 3.3$ Å). Moreover, the fluorine atom is close to a neighboring macrocycle ($d_{F-C} = 1.64$ Å).

The similar crystal packings of (R)-css-2:2, (X)-css-2:2, and (S)-css-2:2 are characterized by the presence of molecular columns running along the a axis, resulting from the head-to-tail packing of complexes generated by simple translations (Figure 8). Parallel columns are stacked along the c axis and lead to an alternate packing of (040) slices of A and B complexes along the [010] direction. Successive (020) layers are antiparallel owing to the 2_1 screw axis running along the crystallographic direction b . The main difference between A and B (040) slices lies in the angle between the pseudo-7-fold molecular axis and the crystallographic direction a , since these two directions are less than 5° apart in complexes A, whereas complexes B are twisted with reference to the a axis by an angle of 37° . This twist generates a free space between complexes B that is partially filled by guest molecules G_B, in particular in the structure of (R)-css-2:2.

Owing to the diversity of inclusion geometries depicted in diastereomerically pure structures, the inclusion features in (X)-css-2:2 are of particular interest, since they should impact the possibility and efficiency of chiral discrimination. During the structural refinement of (X)-css-2:2, location and occupancy factors of the two enantiomers could be established as follows: in complex B, only the (S) enantiomer was detected, whereas both enantiomers are present in complex A, with occupancy factors of 34% for the (S) enantiomer and 66% for the (R) enantiomer. The overall diastereomeric excess is therefore ca. 34% in the (X)-css-2:2 structure, and it is noteworthy from

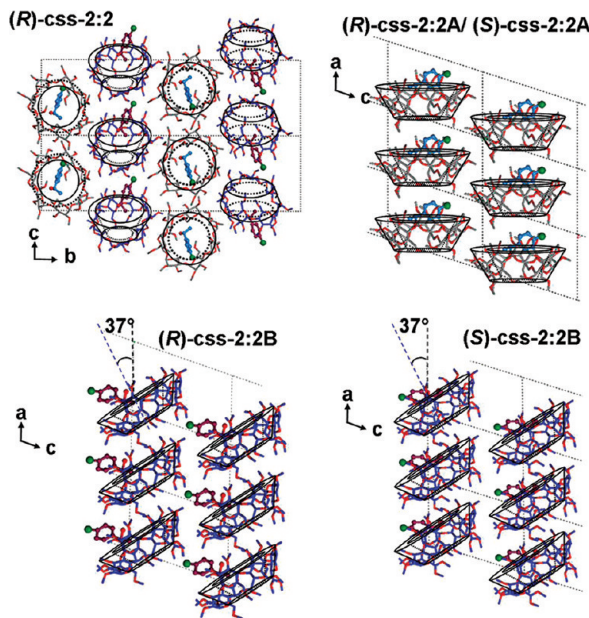


Figure 8. Projection along a of (R)-css-2:2 structure showing the arrangement of molecular layers (040) (upper left) and projections along b of (040) molecular slices in (R)-css-2:2 and (S)-css-2:2 crystal structures. Hydrogen atoms are omitted for clarity.

these results that only macrocycle H_B is selective, in spite of similar macrocyclic conformations. This phenomenon could be due to the different 1D packing observed along the a direction for each macrocycle. Indeed, the empty space induced by the twist of the macrocycle B mentioned above can only be filled by the (R) enantiomer of *p*-F-PE, owing to its unusual inclusion geometry. The crystal is therefore stabilized by the preponderant presence of the (R) enantiomer in the complex B, while the compact packing of the complexes A allows only one inclusion geometry whatever the enantiomer.

3.3.2. Crystal Structures of (R)-pss-M-1:2-H₂O, (X)-pss-O-1:2, and (S)-pss-O-1:2. Up to now, all published crystal structures of host–guest complexes formed with TM β -CD present a (1:1) stoichiometry (Table 2). (R)-pss-M-1:2-H₂O and (S)-pss-O-1:2 therefore constitute the first cases of a (1:2) ratio between host and guest components. Despite this uncommon characteristic, these structures share some features with other complexes reported in the literature, and the macrocycle conformations in (S)-pss-O-1:2 and (R)-pss-M-1:2-H₂O structures are similar to those reported for most structures, with comparable tilt angle values (Supporting Information). However, (R)-pss-M-1:2-H₂O and (S)-pss-O-1:2 are different from one another and are therefore described hereafter separately.

3.3.2.1. Structure of (R)-pss-M-1:2-H₂O. The crystal structure of (R)-pss-M-1:2-H₂O is the ninth occurrence of a P2₁ space group among the 36 crystal structures with TM β -CD reported in Table 2. It belongs to the structural group SGC owing to its space group and crystallographic parameters, but analogies with the structural features of TM β -CD/(R)-*p*-Br-PE can be noticed, in particular in terms of inclusion geometry and presence of a water molecule in the asymmetric unit. The comparison of tilt angles (see the Supporting Information) and superimpositions of TM β -CD molecules revealed that the macrocycle conformation in (R)-pss-M-1:2-H₂O is similar to that existing in structural groups SGA, SGC, and SGD,

confirming the absence of induced fit in these complexes. It appears from Figure 9 that the fluorine atom of G_A is located at

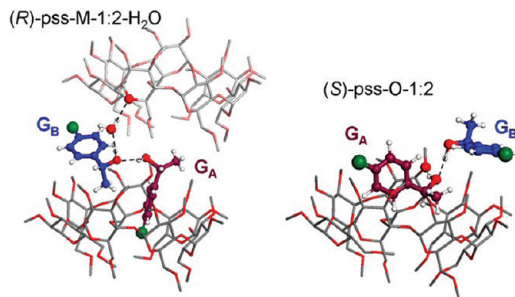


Figure 9. Asymmetric units of (R)-pss-M-1:2-H₂O (left) and (S)-pss-O-1:2 (right) crystal structures. Hydrogen atoms of TM β -CD are omitted for clarity, and in (R)-pss-M-1:2-H₂O, a second macrocycle is shown to highlight the hydrogen bond between the water molecule and this macrocycle.

the bottom of the cavity and its main molecular axis is almost parallel to the pseudo-7-fold axis of TM β -CD, inducing that the major part of the guest molecule A is engulfed in the macrocycle.

By contrast, the second guest (G_B) is not included in the macrocycle but is located upon the border of the TM β -CD macrocycle. In this structure, the main intermolecular interactions are based on hydrogen bonds: the two hydroxyl groups of guest molecules are linked to each other ($d_{O-O} = 2.79$ Å), and the water molecule participates in two hydrogen bonds involving, on the one hand, the guest molecule B ($d_{O-O} = 2.78$ Å) and, on the other hand, an oxygen atom of a neighboring TM β -CD molecule ($d_{O-O} = 2.99$ Å). It can therefore be stated that the water molecule contributes significantly to the structural cohesion of the (R)-pss-M-1:2-H₂O phase, whereas, unexpectedly, no direct hydrogen bond is observed between (R)-*p*-F-PE molecules and the host. It can be argued however that the deep inclusion of G_A in the TM β -CD cavity induces numerous van der Waals contacts.

The crystal packing of (R)-pss-M-1:2-H₂O corresponds to that of SGC structures, and the angle (ca. 24°) between the pseudo-7-fold axis of the cyclodextrin and the crystallographic axis a induces an available space between neighboring complexes. This space is filled by the guest B and by the water molecule, as shown in Figure 10.

3.3.2.2. Structure of (S)-pss-O-1:2. Owing to its space group, crystallographic parameters, and macrocyclic conformation, (S)-pss-O-1:2 belongs to SGA (see Table 2 and Figure 6). Figure 9 shows that one guest molecule (G_A) is partially engulfed in the macrocycle cavity with an inclusion geometry similar to that of (S)-*p*-Br-PE,²⁰ while the second guest (G_B) is located in the free space between neighboring complexes. The inclusion geometry of G_A in (S)-pss-O-1:2 is similar to that depicted in (S)-css-2:2A (Figure 7) ($d_{O-O} = 2.89$ Å), and the two guests are hydrogen bonded to each other by their alcohol function ($d_{O-O} = 2.82$ Å). As in the (R)-pss-M-1:2-H₂O structure, the guest B is located outside the macrocycle, in an interstice between four complexes. Owing to the lack of strong interaction between G_B and TM β -CD, this structure (and that of (R)-pss-M-1:2-H₂O) cannot be described simply as a packing of complexes but more as a “co-crystal”,⁴⁸ made of a 1:1 host–guest association and one *p*-F-PE molecule (Figure 10).

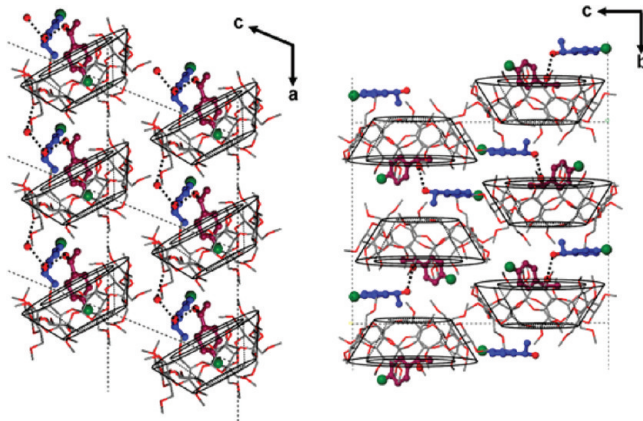


Figure 10. Crystal packings of (R)-pss-M-1:2-H₂O (left) and (S)-pss-O-1:2 (right). Hydrogen atoms are omitted for clarity.

3.3.2.3. Structure of (X)-pss-O-1:2. Using single crystals grown from a racemic solution, the structural determination of (X)-pss-O-1:2 revealed crystal features similar to that depicted for the (S)-pss-O-1:2 structure (see crystallographic parameters and space group, Table 1). Actually the presence of the (R) enantiomer could not be detected during the last refinement steps, in consistency with the similarities observed between (X)-pss-O-1:2 and (S)-pss-O-1:2 XRPD patterns. It can therefore be expected that the pss-O-1:2 phase presents a higher ability for chiral discrimination than css-2:2.

3.4. Various Aspects of a Discussion about Chiral Discrimination. As mentioned above, two different solid phases can be obtained from a racemic solution (css-2:2 and pss-O-1:2) with different abilities for chiral recognition. Owing to its original structural features depicted in the previous section, pss-O-1:2 presumably exhibits a higher potential for chiral discrimination than css-2:2, so efforts have been focused on the study of this former phase and its ability to discriminate enantiomers.

3.4.1. Molecular Modeling and Simulation of Chiral Discrimination. In order to complete the structural study of pss-O-1:2, molecular modeling calculations have been carried out. In a first step, the procedure established by Grandjean et al.²⁰ has been applied to a system formed by one macrocycle and one guest molecule presenting the inclusion geometry observed in (S)-pss-O-1:2, with the aim to estimate the energy involved in the supramolecular association for each enantiomer of *p*-F-PE. In a second step, a study of the impact of the absolute configuration of the guest molecules on the lattice energy of pss-O-1:2 was performed in order to evaluate the stereoselectivity of each crystallographic site in this structure.

In order to assess the stereoselectivity of the cyclodextrin cavity, the energy of host–guest interactions was calculated for each *p*-F-PE enantiomer. The inversion of absolute configuration was performed by a simple permutation of the methyl group and the hydrogen atom of the asymmetric carbon, in order to maintain the hydrogen bonds and the relative host–guest orientation. Thus, the orientation of the main part of the molecule (i.e., the fluorophenyl group) remains also unchanged. The obtained values are given in Figure 11 and show that the interaction is less favorable with the (R) enantiomer by 3.7 kcal·mol⁻¹. Although the simple methodology applied here leads to a probably overestimated energy difference, this result is consistent with the values previously determined by Grandjean et al. for the *p*-Br-PE derivative and

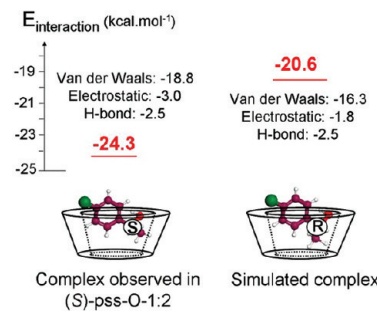


Figure 11. Schematic representation of host–guest complexes observed in (S)-pss-O-1:2 (left) and simulated with the (R) enantiomer (right) with their respective host–guest interaction energies.

indicates that, for this inclusion geometry, the cyclodextrin cavity seems efficient in terms of chiral recognition.

Regarding the energetic contribution of the host–guest complexation to the overall lattice energy and the selectivity of each of the two guest crystallographic sites, the whole (S)-pss-O-1:2 structure was studied with the method described above. After a preliminary energy minimization of the lattice containing two (S) guest enantiomers, one (S) guest was replaced by its counter enantiomer and the geometry optimization was repeated in order to assess the energetic cost of the inclusion of the (R) molecules in the pss-O-1:2 packing.

This energy variation was estimated by calculating the difference between the lattice energy of the resulting simulated structure and the original (S)-pss-O-1:2 structure. The calculated values are shown in Figure 12 and reveal that the

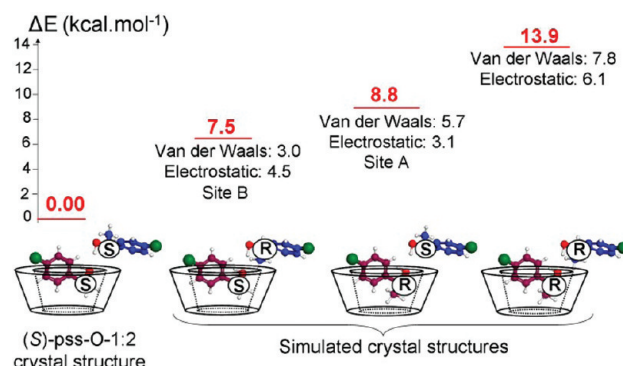


Figure 12. Schematic representation of asymmetric units of (S)-pss-O-1:2 and simulated pss-O-1:2 crystal structures and the corresponding lattice energy variations induced by the presence of the counter enantiomer.

presence of the (R) enantiomer in the structure induces a significant increase of the lattice energy. Moreover, when the inversion of absolute configuration is performed on the enantiomer located either inside (site A) or outside (site B) the cyclodextrin, the energy variations are of the same magnitude (ca. 8 kcal·mol⁻¹), with comparable contributions of van der Waals and electrostatic interactions for these two crystallographic sites. It can be deduced that the presence of a large amount (50% in our simulations) of the “wrong” enantiomer in this crystal structure decreases its stability in such a way that the crystallization of a pss-O-1:2 solid phase significantly enriched with the (R) enantiomer is energetically

unfavored. Since the purpose of this molecular modeling study is not to simulate the existence of solid solutions with a methodological approach similar to that developed by Gervais et al.,⁴⁹ the calculation method applied here (in particular for atomic charges and minimization procedures) cannot be, owing to the molecular size of TM β -CD complexes, as accurate as that used by these authors. However, our (therefore overestimated) values reproduce well the experimental facts, since the simulation of a 50/50 ratio for guest composition is far beyond the de value attainable experimentally for the pss-O-1:2 phase, as shown in the next section (and in Figure 14).

In order to get more insights in the chiral discrimination phenomenon deduced from energy calculations, a direct observation of the steric consequences of the inclusion of the (R) enantiomer in pss-O-1:2 crystal structure has been performed. For this purpose, the van der Waals volume of the molecules can be drawn so as to visualize the guest orientations in the cavities. The clarity of this representation can be enhanced by showing only a suitable 2D section of the structure. Thus, the two cavities A and B can be represented by drawing the intersection between the van der Waals envelope of the molecules in pss-O-1:2 structure and a plane defined by the three relevant chemical substituents (CH₃, OH, and H) bonded to the chiral carbon (Figure 13).

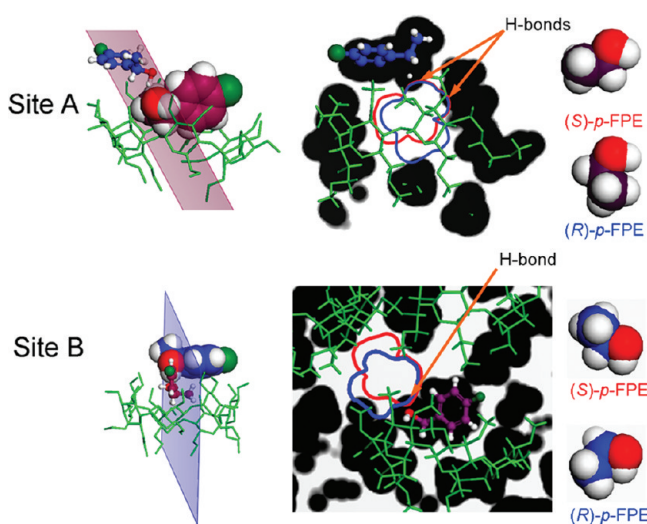


Figure 13. Representation of the intersection between the van der Waals envelopes of the molecules in pss-O-1:2 and the plane defined by the three chemical groups linked to the chiral carbon of the p-F-PE for sites A and B. Free and occupied spaces are represented in white and black, respectively. The van der Waals outlines of the (S) and (R) enantiomers are represented in red and blue, respectively.

The hydrogen bonds described in the structural study of (S)-pss-O-1:2 appear, as expected, as interpenetrations between the van der Waals spheres of the hydroxyl groups of both guests as well as between the included guest and one methoxy group of the cyclodextrin. It appears that the molecular envelope of the (S) enantiomer (drawn in red) do not intersect the van der Waals surfaces of the surrounding molecules, neither in site B nor in site A. As expected, this enantiomer therefore fits both cavities of the structure, whereas, in the case of the (R) enantiomer (obtained according to the procedure described in the molecular modeling study and represented in blue), an interpenetration of the van der Waals surfaces can be seen for both sites with a more pronounced character in the case of site

B. This confirms that the insertion of (R)-p-F-PE molecules in the pss-O-1:2 lattice is unfavored, although a small distortion of the crystal lattice (unfortunately poorly detectable from XRPD patterns) may slightly improve the accommodation of this “wrong” enantiomer.

Hence, this structural approach shows that the two crystallographic sites exhibit an enantioselective character, and indicates that selectivity results from two concomitant contributions: the hydrogen bonds impose the position of the hydroxyl groups, and simultaneously, steric constraints hinder the insertion of the (R) enantiomer in these cavities, in consistency with the molecular modeling results.

3.4.2. Incidence of Crystallization Conditions on Chiral Resolution. From the detailed structural investigations and molecular modeling studies reported above, some assumptions can be readily derived in terms of chiral discrimination capability. The latter was therefore studied experimentally as a function of (i) the host–guest stoichiometry of the solid phase (css-2:2 vs pss-O-1:2), (ii) the enantiomeric composition of the starting solution, and (iii) the kinetic conditions.

Starting from a racemic guest composition and a (1:1) host–guest stoichiometry, crystallization experiments were performed in order to assess the chiral resolution ability of the various solid phases for identical initial supersaturation and temperature ($\beta = 2$ at 35 °C). The measurement of the diastereomeric composition in powders by means of chiral gas chromatography revealed that, as for complexes formed between TM β -CD and other p-X-PE derivatives, enantioenrichment occurs for both phases (X)-css-2:2 and (X)-pss-O-1:2. The diastereomeric excess is not influenced by seeding but appeared to vary strongly from one phase to another: 64% de (S) in (X)-pss-O-1:2 (i.e., ca. 82/18 for the S/R proportion) and 34% de (S) in (X)-css-2:2. These values are consistent with the occupancy rates determined by structural investigations, since a calculated diastereomeric excess of 34% has been observed in (X)-css-2:2 structure, whereas the presence of the (R) enantiomer of p-F-PE (less than 20% in the powder) could not be detected in the (X)-pss-O-1:2 single crystal. Moreover, the significant proportion of (S) enantiomer in the (X)-pss-O-1:2 structure confirms that the chiral discrimination is actually not solely induced by the inclusion phenomenon in the TM β -CD host. Indeed, the maximum diastereomeric excess that can be reached in (X)-pss-O-1:2 is 50% when presuming a complete selectivity of the cyclodextrin cavity and a random insertion of both enantiomers in site B. Since chiral chromatography revealed a diastereomeric excess of 64% in (X)-pss-O-1:2, it is proved that site B is also selective with the same prominent enantiomer and this experimental observation is consistent with the results obtained by molecular modeling and structural studies.

Further crystallization experiments have been performed under the same conditions but starting from solutions with various enantiomeric compositions. The diastereomeric composition of the solid was then plotted as a function of the enantiomeric composition of the solution for css-2:2, pss-O-1:2, and pss-M-1:2-H₂O. The results are presented in Figure 14, in which the black dashed–dotted line represents the composition for which no selectivity is observed ($ee_{\text{solution}} = de_{\text{solid}}$). For the 1:1 solid phase, it can be seen that continuity exists between the enantiopure compositions (blue curve). The css-2:2 phase can therefore crystallize whatever the enantiomeric composition, and this observation is consistent with its solid solution behavior that limits the efficiency of the enantiomeric

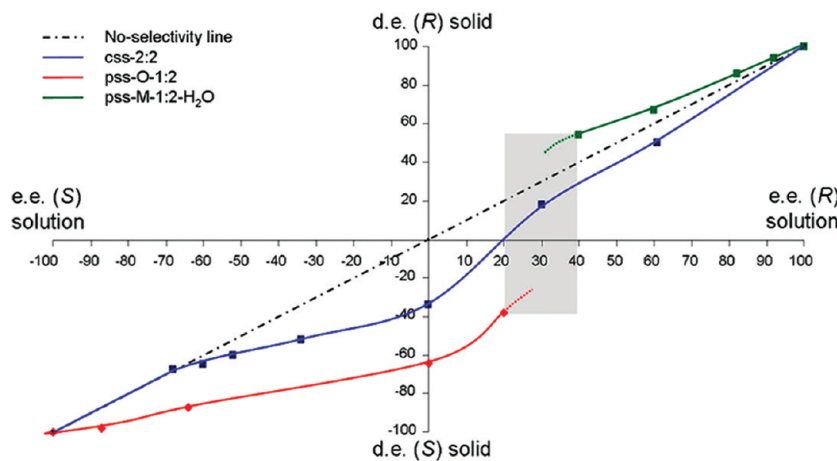


Figure 14. Selectivity of the solid phases as a function of the enantiomeric composition of the starting solution at 35 °C, for a relative initial supersaturation $\beta = 2$ and a 1:1 host–guest stoichiometry. The area of concomitant crystallization of pss-M-1:2-H₂O and pss-O-1:2 is represented in light gray.

separation. On the other hand, pss-O-1:2 and pss-M-1:2-H₂O curves are discontinued and the discrimination ability of pss-M-1:2-H₂O is roughly symmetrical with reference to that of css-2:2 in the accessible composition range. By contrast, pss-O-1:2 presents a significant discrimination, since the red curve is rather far from the no-selectivity line, even for solutions of high enantiopurity.

It should be noticed that, for a solution with an enantiomeric excess in the range 20–40% (R), the coexistence of metastable equilibria induced a concomitant crystallization of both pss-M-1:2-H₂O and pss-O-1:2 and prevented the determination of the diastereomeric composition of each solid phase. Several attempts have been carried out in order to crystallize only one solid phase, but even a combination of seeding and high supersaturation could not ensure the crystallization of a single 1:2 solid phase. Consequently, a mixture of both pss-M-1:2-H₂O and pss-O-1:2 was obtained. Thus, there exists a critical enantiomeric composition of the solution (30% ee (R) \pm 10%) for which the exclusive crystallization of one of the 1:2 solid phases is prevented. These observations highlight the discontinuity existing between the two partial solid solutions and reinforce the statement of diastereomeric behaviors for pss-M-1:2-H₂O and pss-O-1:2.

In order to estimate the influence of kinetics on the ability of TM β -CD to discriminate the enantiomers from a racemic mixture, further crystallization experiments were carried out for each solid phase with different durations, with or without seeding. Unexpectedly, these investigations revealed that the diastereomeric excess remains roughly constant whatever the crystallization duration for each phase: ca. 60% de (S) for (X)-pss-O-1:2 and 30% de (S) for (X)-css-2:2. This observation is poorly consistent with previous results obtained in the homologous series of *p*-X-PE, for which diastereomeric excesses were significantly dependent on durations and kinetic conditions.⁹ Since the diastereomeric composition of the solid sample does not fluctuate during crystallization, it can therefore be assumed that, in the present case, nucleation (rather than kinetic amplification) is the key step that determines the final diastereomeric excess within solid samples. The kinetic factors have consequently a poor influence on the de, and the discrimination in the solid state appears to be mainly determined by thermodynamic parameters, in particular the

solubility limits when the driving force of crystallization is consumed.

3.4.3. Preparative Resolution of Racemic *p*-F-PE. Using the above data, a crystallization procedure was designed in order to separate the enantiomers of *p*-F-PE. Successive recrystallizations were carried out for each solid phase (css-2:2, pss-O-1:2, and pss-M-1:2-H₂O), and solid samples were collected 2 h after the appearance of the first crystals in order to reach a calculated global yield of ca. 50% per crystallization run (Figure 15). It is

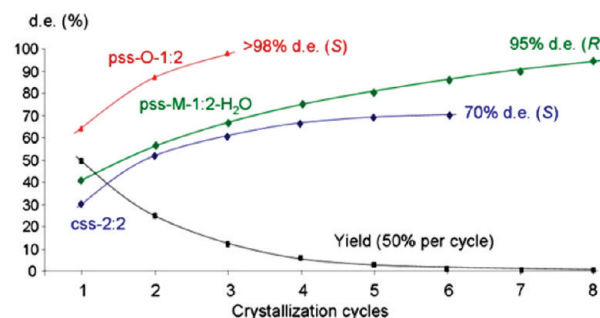


Figure 15. Evolution of the diastereomeric excesses and of the global yield obtained by successive recrystallizations of pss-O-1:2, pss-M-1:2-H₂O, and css-2:2 solid phases.

noteworthy that the first crystallization cycles of css-2:2 and pss-O-1:2 were performed from a true racemic solution, whereas pss-M-1:2-H₂O was obtained from a solution containing an initial enantiomeric excess of 40% (R) (see Figure 14). A sample of high diastereomeric composition (de > 95%) could be obtained after three and eight successive crystallizations for pss-O-1:2 and pss-M-1:2-H₂O, respectively. Conversely, the diastereomeric excess in css-2:2 reaches a plateau at 70% de after five recrystallizations, since the blue curve crosses the no-selectivity line at this particular composition (Figure 14). The difference between these two behaviors is therefore fully consistent with the similarity existing between (R)-css-2:2 and (S)-css-2:2 crystal structures, whereas the discrimination ability of pss-O-1:2 and the structural specificities of pss-M-1:2-H₂O vs pss-O-1:2 in terms of host–guest interactions, hydration state, and crystal packings allow a complete preparative resolution of racemic *p*-F-PE. Due to the stoichiometric difference between the 1:1 and

1:2 phases, it should be noticed that the global yield represented in Figure 15 is calculated by taking into account guest molecules only.

3.4.4. Investigation on the Solvated State. The binding constants in aqueous solution between TM β -CD and the two enantiomers of *p*-F-PE were estimated by ^1H NMR titration. Very small changes of the chemical shifts of macrocycle protons were observed during the titration (ca. $\Delta\delta = -0.03$ ppm), and as a consequence, weak binding constants (with a large uncertainty) were obtained by the Rose–Drago method: $60 \pm 40 \text{ M}^{-1}$ for the TM β -CD/(*S*)-*p*-F-PE complex and $70 \pm 50 \text{ M}^{-1}$ for TM β -CD/(*R*)-*p*-F-PE. Similar results were obtained for TM β -CD/*p*-Br-PE complexes with the exception of H₃ proton, for which a higher shift was measured ($\Delta\delta = -0.1$ ppm),²¹ revealing the inclusion of some *p*-Br-PE molecules inside the TM β -CD cavity. In the case of *p*-F-PE, this interaction could not be demonstrated, indicating that the hypothetical solvated state drawn in Figure 16a is not representative of the solvated state.

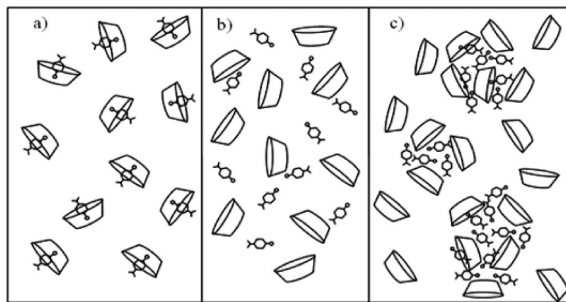


Figure 16. Hypothetical representations of the solvated state based on an inclusion in the host cavity (a); a full miscibility between water and *p*-F-PE (b); a weak binding constant and a poor miscibility between water and *p*-F-PE (c).

However, a fully dissociated state similar to that depicted in Figure 16b seems inconsistent with the poor miscibility observed between water and liquid *p*-F-PE, indicating that guest molecules cannot be solvated by water molecules only. Moreover, the disappearance of the water/*p*-F-PE emulsion in the presence of one equivalent of TM β -CD implies particular interactions in solution between host and guest molecules, probably able to prevent direct contacts between water and the hydrophobic part of *p*-F-PE molecules. In order to fulfill these two conditions (weak binding constants and disappearance of the emulsion in the presence of 1 equiv of TM β -CD), a third hypothetical solvated state can be proposed (Figure 16c). This hypothesis relies on the existence of molecular clusters consisting of $(\text{p-F-PE})_x (\text{TM}\beta\text{-CD})_y$ aggregates with $x \geq y$. In the clusters, a minor proportion of guest molecules is engulfed in the host cavity (accounting for the low binding constants), and direct *p*-F-PE/water interactions can be avoided. The unusual stoichiometries observed in pss-O-1:2 and pss-M-1:2-H₂O solid phases can then be explained by assuming that a significant proportion of TM β -CD molecules is not involved in the postulated clusters (i.e., $x > y$). It can also be speculated that, for racemic guest composition in solution, these clusters are enriched with the (*S*) enantiomer, which would account for the high enantioenrichments obtained upon crystallization, whereas solvated complexes containing (*R*) guest enantiomers would remain in solution (owing to their higher solubility, see Figure 5) or could have their nucleation inhibited.⁵⁰

As illustrated in Figure 17, pss-M-1:2-H₂O and pss-O-1:2, consisting of metastable solid phases, are supposed to be more

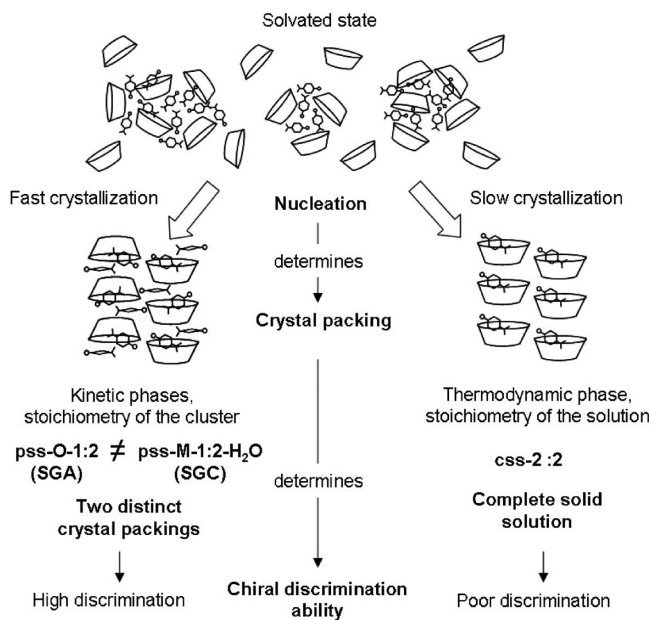


Figure 17. Summary of the relationships between the solid phases and the starting solvated state (1:1 stoichiometry and racemic guest composition) as a function of the experimental conditions.

representative of the solvated state. Thus, a fast crystallization from the hypothetical solvated state drawn in Figure 16c could induce the nucleation and growth of crystal packings containing 1:2 host–guest ratios with a rather high chiral discrimination. On the other hand, the implementation of smooth crystallization conditions (or suitable seeding or suspending the kinetic crystal forms) generates, in consistency with the Ostwald rule of stages,⁵¹ the formation of the lower-solubility phase exhibiting, owing to its structural features, a lower ability for chiral discrimination.

3.4.5. Mechanism of Chiral Discrimination. The structural study of pss-O-1:2 combined with molecular modeling calculations and the physical characterizations of solid samples have highlighted the occurrence of a chiral discrimination for guest molecules that are not included in the cyclodextrin cavity. This result is in opposition with previous studies stating that a high chiral discrimination is usually ensured by significant interactions between the guest molecule and the inner part of TM β -CD.^{10,13,15,20} In these studies, the enantiomeric recognition was assumed to result from hydrogen bonds and van der Waals interactions but also from steric factors such as the presumed “induced fit” of the cyclodextrin macrocycle through the “lock and key” concept. In this widespread approach, the possibility of resolving a racemic mixture of guest molecules is described as a direct consequence of differences between the inclusion geometries of the two enantiomers in the cyclodextrin cavity. In the case of *p*-F-PE, the chiral discrimination does not rely solely on such a condition and appears to be related to the selectivity and the structural features of the crystallographic sites occupied by each guest enantiomer. Hence, one has to consider not only the interaction between the host cavity and the guest molecule but also the discrimination ability of the crystal packings.²¹ In pss-O-1:2, the chiral selectivity results from a hybrid mechanism involving an interplay between two

contributions: (i) a molecular contribution where the discrimination is ensured by the cyclodextrin cavity as demonstrated in the literature;¹³ (ii) a supramolecular contribution in which the whole crystal packing acts as the host entity. This type of chiral selectivity by a host lattice, extensively described in the literature as “resolution by lattice inclusion”,^{2–4,52–54} had not yet been evidenced in the case of cyclodextrin complexes. In this particular type of resolution, the asymmetry of the cavities is induced by the packing of host molecules. The inclusion phenomenon results from the insertion of guest molecules into the host lattice during the crystallization, and the segregation between the two guest enantiomers is mainly based on several contributions such as hydrogen bonds, van der Waals interactions, and steric complementarity between the shape and size of the cavity and that of the enantiomers. All of these parameters were shown to be responsible for the selectivity of site B in pss-O-1:2 crystal structure, thus confirming the relevance of this approach for the rationalization of the chiral discrimination mechanism in such a solid phase.

4. CONCLUSION

Various solid phases have been identified in the system TM β -CD/(\pm)*p*-F-PE/water, each of them presenting a distinct solid solution behavior as a function of the enantiomeric composition. Two metastable phases, namely, pss-M-1:2-H₂O and pss-O-1:2, consist of diastereomeric partial solid solutions with a 1:2 host–guest stoichiometry, whereas the stable phase is a complete solid solution labeled css-2:2. The disparities between their chiral discrimination efficiency were analyzed on the basis of structural features, and since no chiral discrimination could be evidenced in the solvated state, it can be postulated that the chiral segregation is predominantly determined by the structural features of the solid phase that nucleates and grows. In particular, it is evidenced that the usual hypothesis about a pre-existing molecular inclusion in solution, induced by hydrophobic interactions, is not validated in the present case. Indeed, it is shown that the existence of solvated molecular clusters is the only hypothesis consistent with the poor binding constants and the unusual stoichiometries observed in this system.

The detailed structural analyses of pss-M-1:2-H₂O and pss-O-1:2 have demonstrated that these crystalline phases can be described as cocrystals formed between a host–guest inclusion complex plus a crystal lattice guest molecule. Moreover, the combination of structural studies and molecular modeling calculation has shown that a significant selectivity can be observed outside the cyclodextrin cavity. Indeed, an important chiral recognition has been evidenced for guest molecules that are not included in the macrocycle but located in lattice cavities induced by the stacking of TM β -CD molecules. This original result contradicts the general assumption formulated, for instance, by Harata, stating that the ability of cyclodextrins for chiral discrimination is ensured by their intrinsic cavity, without considering the contribution of the crystal lattice. Our analysis suggests that the cavities induced by the packing of the macrocycles or by (1:1) complexes have also to be taken into account, and this new approach, in which the chiral discrimination is considered both at the supramolecular and at the lattice levels, allows the rationalization of the unusual behavior of the complexes formed between TM β -CD and the enantiomers of *p*-F-PE.

Hence, the chiral discrimination observed in these solid phases results from an interplay between supramolecular inclusion in the cyclodextrin cavity and lattice inclusion. To our knowledge, this system constitutes the first report of this kind of hybrid mechanism.

■ ASSOCIATED CONTENT

S Supporting Information

A cif file containing the six crystal structures. Representations of thermal motions for the six asymmetric units. Table with full data for the 36 entries gathered in Table 2. This material is available free of charge via the Internet at <http://pubs.acs.org>.

■ AUTHOR INFORMATION

Corresponding Author

*Phone: +33 2 35 52 24 28. Fax: +33 2 35 52 29 59. E-mail: samuel.petit@univ-rouen.fr.

Present Address

[†]Analytical R&D, Novartis Pharma AG, Basel, Switzerland.

Notes

The authors declare no competing financial interest.

■ ACKNOWLEDGMENTS

The French Ministry of Research is acknowledged for financial support to Y.A. via the E.D. n°351 (SPMII).

■ LIST OF ABBREVIATIONS

CD, cyclodextrin
TM β -CD, permethylated β -cyclodextrin
<i>p</i> -X-PE, 1-(<i>p</i> -halogenophenyl)ethanol
ee, enantiomeric excess
de, diastereomeric excess
(<i>R</i>)-css-2:2, complete solid solution with 1:1 host guest stoichiometry, containing pure (<i>R</i>)- <i>p</i> -F-PE
(<i>S</i>)-css-2:2, complete solid solution with 1:1 host guest stoichiometry, containing pure (<i>S</i>)- <i>p</i> -F-PE
(<i>X</i>)-css-2:2, complete solid solution with 1:1 host guest stoichiometry, containing 67% (<i>S</i>)- <i>p</i> -F-PE
(<i>R</i>)-pss-M-1:2-H ₂ O, monohydrated monoclinic partial solid solution with a 1:2 host–guest stoichiometry containing pure (<i>R</i>)- <i>p</i> -F-PE
(<i>S</i>)-pss-O-1:2, orthorhombic partial solid solution with a 1:2 host–guest stoichiometry containing pure (<i>S</i>)- <i>p</i> -F-PE
(<i>X</i>)-pss-O-1:2, orthorhombic partial solid solution with a 1:2 host–guest stoichiometry containing 82% (<i>S</i>)- <i>p</i> -F-PE

■ REFERENCES

- (a) Coquerel, G. In *Topics in Current Chemistry (Novel Optical Resolution Technologies)*; Sakai, K., Hirayama, N., Tamura, R., Eds.; Springer: Berlin, Heidelberg, 2007; Vol. 269, Chapter 1, pp 1–50.
(b) Kellogg, R. M. *Synthesis* **2003**, *10*, 1626–1638. (c) Fogassy, E.; Nogradi, M.; Palovics, E.; Schindler, J. *Synthesis* **2005**, *36*, 1555–1568.
- (2) Urbanczyk-Lipkowska, Z.; Toda, F. In *Separations and reactions in organic supramolecular chemistry*; Toda, F., Bishop, R., Eds.; J. Wiley & Sons: New York, 2004; Chapter 1.
- (3) Nemak, K.; Acs, M.; Jaszay, Z. M.; Kozma, D.; Fogassy, E. *Tetrahedron* **1996**, *52*, 1637–1642.
- (4) Arad-Yellin, R.; Green, B. S.; Knossow, M.; Tsoucaris, G. *J. Am. Chem. Soc.* **1983**, *105*, 4561–4571.
- (5) Wenz, G. *Angew. Chem., Int. Ed. Engl.* **1994**, *33*, 803–822.
- (6) Liu, L.; Guo, Q. X. *J. Inclusion Phenom. Macrocyclic Chem.* **2002**, *42*, 1–14.

- (7) Mikolajczyk, M.; Drabowicz, J. *J. Am. Chem. Soc.* **1978**, *100*, 2510–2515.
- (8) Saenger, W. *Angew. Chem., Int. Ed. Engl.* **1980**, *19*, 344–362.
- (9) Grandeury, A.; Tisse, S.; Gouhier, G.; Agasse, V.; Petit, S.; Coquerel, G. *Chem. Eng. Technol.* **2003**, *26*, 354–358.
- (10) Makedonopoulou, S.; Yannakopoulou, K.; Mentzafos, D.; Lamzin, V.; Popov, A.; Mavridis, I. M. *Acta Crystallogr.* **2001**, *B57*, 399–409.
- (11) Hamilton, J. A.; Chen, L. *J. Am. Chem. Soc.* **1988**, *110*, 5833–5841.
- (12) Hamilton, J. A.; Chen, L. *J. Am. Chem. Soc.* **1988**, *110*, 4379–4391.
- (13) Harata, K. *Chem. Rev.* **1998**, *98*, 1803–1827.
- (14) Caira, M. R.; Griffith, V. J.; Nassimbeni, L. R. *J. Inclusion Phenom.* **1995**, *20*, 277–290.
- (15) Kano, K.; Kato, K. Y.; Kodera, M. *J. Chem. Soc., Perkin Trans. 2* **1996**, *1211*–1217.
- (16) Harata, K.; Uekama, K.; Otagiri, M.; Hirayama, F. *Bull. Chem. Soc. Jpn.* **1983**, *56*, 1732–1736.
- (17) Tsorteki, F.; Bethanis, K.; Mentzafos, D. *Carbohydr. Res.* **2004**, *339*, 233–240.
- (18) Ferron, L.; Guillen, F.; Coste, S.; Coquerel, G.; Plaquevent, J. C. *Chirality* **2006**, *18*, 662–666.
- (19) Cruickshank, D.; Rougier, N. M.; Vico, R. V.; de Rossi, R. H.; Bujan, E. I.; Bourne, S. A.; Caira, M. R. *Carbohydr. Res.* **2010**, *345*, 141–147.
- (20) Grandeury, A.; Petit, S.; Gouhier, G.; Agasse, V.; Coquerel, G. *Tetrahedron: Asymmetry* **2003**, *14*, 2143–2152.
- (21) Grandeury, A.; Condamine, E.; Hilfert, L.; Gouhier, G.; Petit, S.; Coquerel, G. *J. Phys. Chem. B* **2007**, *111*, 7017–7026.
- (22) Rose, N. J.; Drago, R. S. *J. Am. Chem. Soc.* **1959**, *81*, 6138–6141.
- (23) SMART for WNT/2000 V5.622 (2001), Smart software reference manual, Bruker Advanced X Ray Solutions, Inc., Madison, Wisconsin, USA.
- (24) SAINT+ V6.02 (1999), Saint software reference manual, Bruker Advanced X Ray Solutions, Inc., Madison, Wisconsin, USA.
- (25) WinGX: Version 1.70.01: An integrated system of Windows Programs for the solution, refinement and analysis of Single Crystal X-Ray Diffraction Data, By Farrugia, L. *J. J. Appl. Crystallogr.* **1999**, *32*, 837–838.
- (26) Included in WinGX suite: SHELXD- A program for crystal structure solution, G. M. Sheldrick, University of Goettingen, Germany, 2002.
- (27) Included in WinGX suite: SHELXL-97—a program for crystal structure refinement, Sheldrick, G. M., University of Goettingen, Germany, 1997, release 97-2.
- (28) Shi, J.; Guo, D. S.; Ding, F.; Liu, Y. *Eur. J. Org. Chem.* **2009**, 923–931.
- (29) Dean, P. M. *Aust. J. Chem.* **2007**, *60*, 133–138.
- (30) Stellenboom, N.; Hunter, R.; Caira, M. R.; Bourne, S. A.; Cele, K.; Qwebani, T.; le Roex, T. *ARKIVOC* **2007**, *8*, 53–63.
- (31) Caira, M. R.; Hunter, R.; Bourne, S. A.; Smith, V. J. *Supramol. Chem.* **2004**, *16*, 395–403.
- (32) Harata, K.; Uekama, K.; Imai, T.; Hirayama, F.; Otagiri, M. *J. Inclusion Phenom.* **1988**, *6*, 443–460.
- (33) Harata, K.; Hirayama, F.; Arima, H.; Uekama, K.; Miyaji, T. *J. Chem. Soc., Perkin Trans. 2* **1992**, 1159–1166.
- (34) Mentzafos, D.; Mavridis, I. M.; Schenk, H. *Carbohydr. Res.* **1994**, *253*, 39–50.
- (35) Brown, G. R.; Caira, M. R.; Nassimbeni, L. R.; van Oudtshoorn, B. *J. Inclusion Phenom.* **1996**, *26*, 281–294.
- (36) Cruickshank, D.; Bourne, S. A.; Caira, M. R. *ARKIVOC* **2011**, 103–115.
- (37) Rontogianni, A.; Mavridis, I. M.; Israel, R.; Beurskens, G. J. *Inclusion Phenom. Mol. Recognit. Chem.* **1998**, *32*, 415–428.
- (38) Cardinael, P.; Peulon, V.; Perez, G.; Coquerel, G.; Toupet, L. J. *Inclusion Phenom. Macrocyclic Chem.* **2001**, *39*, 159–167.
- (39) Caira, M. R.; Giordano, F.; Vilakazi, S. L. *Supramol. Chem.* **2004**, *16*, 389–393.
- (40) Mieusset, J. L.; Krois, D.; Pacar, M.; Brecker, L.; Giester, G.; Brinker, U. H. *Org. Lett.* **2004**, *6*, 1967–1970.
- (41) Caira, M. R.; Griffith, V. J.; Nassimbeni, L. R.; van Oudtshoorn, B. *Supramol. Chem.* **1996**, *7*, 119–124.
- (42) Balula, S. S.; Coelho, A. C.; Braga, S. S.; Hazell, A.; Valente, A. A.; Pillinger, M.; Seixas, J. D.; Romao, C. C.; Goncalves, I. S. *Organometallics* **2007**, *26*, 6857–6863.
- (43) Caira, M. R.; Bourne, S. A.; Vilakazi, S. L.; Reddy, L. *Supramol. Chem.* **2004**, *16*, 279–285.
- (44) Caira, M. R.; Griffith, V. J.; Nassimbeni, L. R.; van Oudtshoorn, B. *J. Chem. Soc., Perkin Trans. 2* **1994**, 2071–2072.
- (45) Pereira, C. C. L.; Nolasco, M.; Braga, S. S.; Almeida Paz, F. A.; Ribeiro Claro, P.; Pillinger, M.; Goncalves, I. S. *Organometallics* **2007**, *26*, 4220–4228.
- (46) Caira, M. R.; Bourne, S. A.; Mhlongo, W. T.; Dean, P. M. *Chem. Commun.* **2004**, 2216–2217.
- (47) Tsorteki, F.; Bethanis, K.; Pinotsis, N.; Giastas, P.; Mentzafos, D. *Acta Crystallogr., Sect. B* **2005**, *61*, 207–217.
- (48) Wouters, J.; Quéré, L., Eds. *Pharmaceutical salts and cocrystals*; RSC Publishing: Cambridge, U.K., 2012.
- (49) Gervais, C.; Grimbergen, R. F. P.; Markovits, I.; Ariaans, G. J. A.; Kaptein, B.; Bruggink, A.; Broxterman, Q. B. *J. Am. Chem. Soc.* **2004**, *126*, 655–662.
- (50) Leeman, M.; Brasile, G.; Gelens, E.; Vries, T.; Kaptein, B.; Kellogg, R. *Angew. Chem., Int. Ed.* **2008**, *47*, 1287–1290.
- (51) Threlfall, T. *Org. Process Res. Dev.* **2003**, *7*, 1017–1027.
- (52) Toda, F. *Aust. J. Chem.* **2001**, *54*, 573–582.
- (53) Toda, F. *Enantiomer Separation: Fundamental and Practical Methods*; Kluwer Academic Publisher: Dordrecht, The Netherlands, 2004; Chapter 1, pp 1–47.
- (54) Müller, S.; Cyrus Afraz, M.; de Gelder, R.; Ariaans, G. J. A.; Kaptein, B.; Broxterman, Q. B.; Bruggink, A. *Eur. J. Org. Chem.* **2005**, 1082–1096.